

## ON THE CHOICE OF WAVESPEEDS FOR THE HLLC RIEMANN SOLVER\*

P. BATTEN<sup>†</sup>, N. CLARKE<sup>‡</sup>, C. LAMBERT<sup>§¶</sup>, AND D. M. CAUSON<sup>§</sup>

**Abstract.** This paper considers a class of approximate Riemann solver devised by Harten, Lax, and van Leer (denoted HLL) for the Euler equations of inviscid gas dynamics. In their 1983 paper, Harten, Lax, and van Leer showed how, with a priori knowledge of the signal velocities, a single-state approximate Riemann solver could be constructed so as to automatically satisfy the entropy condition and yield exact resolution of isolated shock waves. Harten, Lax, and van Leer further showed that a two-state approximation could be devised, such that both shock and contact waves would be resolved exactly. However, the full implementation of this two-state approximation was never given. We show that with an appropriate choice of acoustic and contact wave velocities, the two-state so-called HLLC construction of Toro, Spruce, and Speares will yield this exact resolution of isolated shock and contact waves. We further demonstrate that the resulting scheme is positively conservative. This property, which cannot be guaranteed by any linearized approximate Riemann solver, forces the numerical method to preserve initially positive pressures and densities. Numerical examples are given to demonstrate that the solutions generated are comparable to those produced with an exact Riemann solver, only with a stronger enforcement of the entropy condition across expansion waves.

**Key words.** approximate Riemann solvers, HLL, HLLC, wavespeed estimates

**AMS subject classifications.** 35L, 65C

**PII.** S1064827593260140

**1. Introduction.** In 1959, Godunov [5] presented a first-order upwind scheme which could capture shock waves without introducing spurious oscillations. Godunov's method and its various derivatives have since gained increasing popularity due to their robustness and ability to achieve high resolution of stationary discontinuities. Central to these methods is the exact or approximate solution of the Riemann problem. It has long been argued that exact Riemann solutions are too expensive or involve an unnecessary amount of detail for most numerical methods of the Godunov type. More significantly, an implicit numerical method requires a differentiable flux in order to arrive at a linearized (hence easily solvable) set of algebraic equations at each time-step or iteration. However, the exact solution is not available in any closed form. As a result, a new area developed in the field of designing approximate solutions to the Riemann problem [11, 12, 8, 3, 4, 15]. Many of these resulting upwind schemes are capable of producing good results on specific problems, but certain approximations can also fail dramatically or produce spurious numerical side effects. This paper considers a simple class of approximate Riemann solvers devised by Harten, Lax, and van Leer [8] (HLL) which have proved extremely reliable and robust. These approximate solutions are constructed by averaging intermediate states in the exact

---

\*Received by the editors December 15, 1993; accepted for publication (in revised form) March 20, 1996.

<http://www.siam.org/journals/sisc/18-6/26014.html>

<sup>†</sup>Department of Mechanical Engineering, Thermofluids Division, UMIST, Sackville Street, Manchester, M60 1QD, UK (Paul.Batten@umist.ac.uk). Part of this work was carried out while the first author was employed on an EPSRC-funded research project at the Manchester Metropolitan University.

<sup>‡</sup>Department of Aeronautics and Astronautics, Southampton University, Southampton, UK.

<sup>§</sup>Department of Mathematics and Physics, Manchester Metropolitan University, Manchester, M1 5GD, UK (C.Lambert@ex.ac.uk).

<sup>¶</sup>Current address: Department of Computer Science, University of Exeter, Exeter, UK.

solution, while respecting certain design principles which guarantee an accurate and convergent Godunov-type method.

The simplest HLL approximation assumes only one intermediate wave state between the two acoustic waves. This solver has proved extremely popular and, with an appropriate choice of wave velocities, satisfies all the required design principles bar one: it cannot exactly resolve isolated contact discontinuities. Harten, Lax, and van Leer [8] further demonstrated that a two-state approximation could exist, which would yield exact resolution of both shock and contact waves. However, the full implementation of this was never given. A breakthrough in this area came from Toro, Spruce, and Speares [15], who showed that a simple two-state solution (denoted HLLC) could be generated directly by making an assumption on the particle velocity in the Riemann fan. In the present paper, we suggest algorithms for computing the wavespeeds required by HLLC. We show that the resulting numerical method resolves isolated shock and contact waves exactly and is positively conservative. Finally, we present a small number of numerical examples, including comparisons with solutions obtained using the exact Riemann solver.

**2. Godunov-type methods and upstream differencing.** In this paper we consider numerical methods suitable for the solution of nonlinear advection problems, such as the following scalar wave equation:

$$(1) \quad u_t + f(u)_x = 0, \quad u(x, 0) = u_o(x),$$

where  $u$ ,  $f$ ,  $t$ , and  $x$  represent the transported variable, its (convex) flux function, time, and distance, respectively.

To allow for discontinuities, we consider weak solutions of (1) that satisfy

$$(2) \quad \int_0^\infty \int_{-\infty}^\infty [w_t u + w_x f(u)] dx dt + \int_{-\infty}^\infty w(x, 0) u_o(x) dx = 0$$

for test functions  $w(x, t)$  of compact support. The above condition is equivalent to requiring that the following integral of equation (1) hold over an arbitrary rectangle:

$$(3) \quad \int_a^b u(x, \Delta t) dx - \int_a^b u(x, 0) dx + \int_0^{\Delta t} f(u(b, t)) dt - \int_0^{\Delta t} f(u(a, t)) dt = 0.$$

We say that  $u$  is a weak solution of (1) iff  $u$  satisfies (1) pointwise in each smooth region and the Rankine–Hugoniot jump condition

$$(4) \quad f(u_r) - f(u_l) = s(u_r - u_l)$$

across any discontinuities. Here  $s$  is the speed of propagation of the discontinuity and  $u_l$  and  $u_r$  are the states to the left and right of the discontinuity. It is known that weak solutions of (1) are not uniquely determined by their initial data. The physically relevant solution is given by the limit solution, as  $\epsilon \downarrow 0$ , of the viscous equation

$$(5) \quad u_t + f(u)_x = \epsilon u_{xx}.$$

In such limit solutions, signals can only converge on a discontinuity; that is, signals will not diverge from a physical shock (see Lax [9]).

The starting point for our numerical scheme follows Godunov [5] in first dividing the solution domain into cells, over each of which  $u(x)_i$  takes a different, piecewise

constant value. This solution may be integrated in time using, for example, a forward Euler time-stepping scheme,

$$(6) \quad u_i^{n+1} = u_i^n - \frac{\Delta t}{\Delta x} (h_{i+\frac{1}{2}}^n - h_{i-\frac{1}{2}}^n).$$

Provided the numerical flux function,  $h(u)$ , is consistent with the original flux function  $f(u)$ , in the sense that

$$(7) \quad h(u, u \dots u) = f(u),$$

then scheme (6) is said to be in conservation form and the numerical solution will be a weak solution of (1).

The simplest first-order upwind scheme, due to Courant, Isaacson, and Rees (CIR) [2], is given by (6) with the numerical flux defined from

$$(8) \quad h(u)_{i+\frac{1}{2}}^n = \max \left[ 0, (f_u)_{i+\frac{1}{2}} \right] u_i + \min \left[ 0, (f_u)_{i+\frac{1}{2}} \right] u_{i+1},$$

where  $f_u$  is identified as the wavespeed and the max, min functions determine the upwind flux from the direction of the wave. In the above form, however, this scheme does not distinguish between physically admissible (given by the limit solution (5)) and inadmissible discontinuities. The difficulty stems from the ambiguity of having to choose a single representative wavespeed,  $f_u$ , from a region (such as an expansion fan) which may contain a continuous transition of wave velocity. One possible remedy is to prevent the numerical approximation to the wavespeed at the interface from going to zero, whenever it is less than some measure of the spreading rate of the wave,  $\sigma_s$ . This provides sufficient viscosity to prevent nonphysical shocks from forming. A suitable expression for  $\sigma_s$  was suggested by Harten and Hyman [6], as

$$(9) \quad (\sigma_s)_{i+\frac{1}{2}} = \max[0, (f_u)_{i+1} - (f_u)_{i+\frac{1}{2}}, (f_u)_{i+\frac{1}{2}} - (f_u)_i].$$

This term is positive across rarefaction waves, but unlike classical artificial viscosity, it goes to zero across shock waves. The interface flux in (6) can then be written

$$(10) \quad h(u)_{i+\frac{1}{2}}^n = \max \left[ 0, (\sigma_s)_{i+\frac{1}{2}}, (f_u)_{i+\frac{1}{2}} \right] u_i + \min \left[ 0, -(\sigma_s)_{i+\frac{1}{2}}, (f_u)_{i+\frac{1}{2}} \right] u_{i+1}.$$

For a system of equations, a number of waves of differing strengths may be traveling at different speeds. The system

$$(11) \quad U_t + F(U)_x = 0$$

may be rewritten as

$$(12) \quad U_t + A(U)U_x = 0,$$

where  $A(U)$  is the Jacobian matrix,  $\partial F / \partial U$ . This system is called hyperbolic if the eigenvalues of  $A$  are real and each corresponding eigenvector is linearly independent. Consider the one-dimensional initial value problem with constant but differing left and right states

$$(13) \quad U(x, 0) = \begin{cases} U_l & \text{if } x < 0, \\ U_r & \text{if } x \geq 0. \end{cases}$$

The Riemann problem is the initial value problem (11), (13) consisting of the break-up of this single discontinuity. Its solution, denoted by  $R(x/t; U_l, U_r)$ , depends only on the states  $U_l, U_r$  and the ratio  $x/t$ .

Godunov's scheme [5] considers piecewise constant states in each mesh cell, with discontinuities at each cell interface. The exact solution to the Riemann problem is found at each interface, and a new cell average value,  $U_i^{n+1}$ , is obtained by averaging the solutions over the control volume

$$(14) \quad U_i^{n+1} = \frac{1}{\Delta x} \int_{i-\frac{1}{2}}^i R(x/t, U_{i-1}^n, U_i^n) dx + \frac{1}{\Delta x} \int_i^{i+\frac{1}{2}} R(x/t, U_i^n, U_{i+1}^n) dx.$$

Since  $R^n$  satisfies the conservation law (3), the above integral can be evaluated over the rectangle  $(i - \frac{1}{2}, i + \frac{1}{2}) \times (0, \Delta t)$ , yielding the equivalent result:

$$(15) \quad U_i^{n+1} = U_i^n - \frac{\Delta t}{\Delta x} [F(R(0, U_{i-1}^n, U_i^n)) - F(R(0, U_i^n, U_{i+1}^n))],$$

where  $R(0, U_l, U_r)$  is the solution to the Riemann problem at the interface between states  $U_l$  and  $U_r$ . Scheme (15) is the system equivalent to the CIR scheme (6), with the interface flux defined by the exact Riemann solution  $R(0, U_l, U_r)$ .

Harten, Lax, and van Leer [8] show that any Godunov-type scheme can be expressed in conservation form, with a numerical flux,  $F_{lr}(U_l, U_r)$ , determined by applying the integral conservation law (3) over the rectangle  $(i - \frac{1}{2}, i) \times (0, \Delta t)$ . This gives

$$(16) \quad \int_{i-1}^{i-\frac{1}{2}} w(x/t; U_l, U_r) dx - \frac{\Delta x}{2} U_l + \Delta t (F_{lr} - F_l) = 0,$$

where  $w(x/t; U_l, U_r)$  is the exact or approximate solution to the Riemann problem. Equation (16) may be rearranged to give

$$(17) \quad F_{lr} = F_l - \frac{1}{\Delta t} \int_{i-1}^{i-\frac{1}{2}} w(x/\Delta t; U_l, U_r) dx + \frac{\Delta x}{2\Delta t} U_l.$$

Equation (17) is subsequently used to construct numerical fluxes,  $F_{lr}$ , based on the averaged-state approximations of Harten, Lax, and van Leer [8].

**3. HLL approximate Riemann solvers.** In 1983, Harten, Lax, and van Leer [8] presented a new approach to solving the Riemann problem approximately. The resulting methods have become known as HLL Riemann solvers. Whereas the exact Riemann solution contains a large amount of detail, the HLL solvers assume fewer intermediate wave states, by averaging sections of the exact solution over the Riemann fan.

In the case of the Euler equations, the solution to the Riemann problem consists of a contact wave and two acoustic waves, which may be either shocks or expansion fans (see Figure 1). If the fastest-moving wave (with velocity denoted by  $S_R$ ) is an expansion, then region 5 represents a continuous transition from states 4 to 6, otherwise the wave is a shock representing a single discontinuous jump from states 4 to 6, and region 5 does not exist. The middle wave, separating states 3 and 4, is the contact wave, whose velocity is denoted by  $S_M$ . The acoustic waves have the smallest and largest velocities ( $S_L, S_R$ , respectively) of all the waves present in the exact solution. If  $S_L > 0$ , then the flow is supersonic from left to right and the

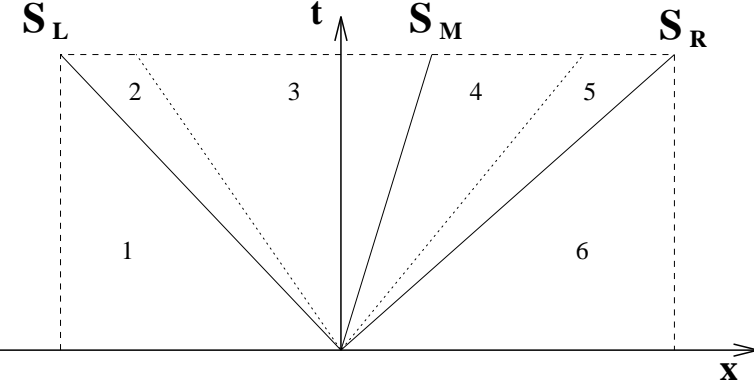


FIG. 1. General Riemann fan for the Euler equations.

upwind flux is simply defined from  $F = F(U_l)$  where  $U_l$  is the state to the left of the discontinuity. If  $S_R < 0$ , then the flow is supersonic from right to left and the flux is defined from  $F = F(U_r)$  where  $U_r$  is the state to the right of the discontinuity. We now consider two approaches for calculating the flux  $F_{lr}^*(U_l, U_r)$  in the more difficult subsonic case, when  $S_L < 0 < S_R$ . The actual calculation of these wavespeeds will be discussed later in some detail.

**3.1. The HLL flux.** The three-dimensional Euler equations may be written in integral form as

$$(18) \quad \oint [U dx - F(U) dt] = 0,$$

where

$$(19) \quad U = \begin{bmatrix} \rho \\ \rho u \\ \rho v \\ \rho w \\ e \end{bmatrix}, \quad F = \begin{bmatrix} \rho q \\ \rho uq + pn_x \\ \rho vq + pn_y \\ \rho wq + pn_z \\ (e + p)q \end{bmatrix},$$

where  $\rho$ ,  $u$ ,  $v$ ,  $w$ ,  $e$ , and  $p$  represent density, Cartesian velocity components, total energy per unit volume, and pressure, respectively. The directed velocity,  $q = un_x + vn_y + wn_z$ , is the component of velocity acting in the  $\vec{n}$  direction, where the unit vector  $\vec{n}$  gives the orientation of the membrane or interface separating the two states which define this Riemann problem. Note that although (18) and Figure 2 illustrate the specific case,  $\vec{n} = [1, 0, 0]^T$ , the results hold for arbitrary  $\vec{n}$ . In a general two- or three-dimensional finite volume framework, one has simply to scale the flux per unit area by the appropriate interface area.

If the flow is subsonic, then a simple approximate Riemann solution can be obtained by ignoring the contact discontinuity and assuming a single, averaged intermediate state,  $U^*$ , between the two acoustic waves,  $S_L, S_R$  (see Figure 2). The single-state approximate Riemann solution was defined by Harten, Lax, and van Leer [8] as

$$(20) \quad U_{HLL} = \begin{cases} U_l & \text{if } S_L > 0, \\ U^* & \text{if } S_L \leq 0 \leq S_R, \\ U_r & \text{if } S_R < 0. \end{cases}$$

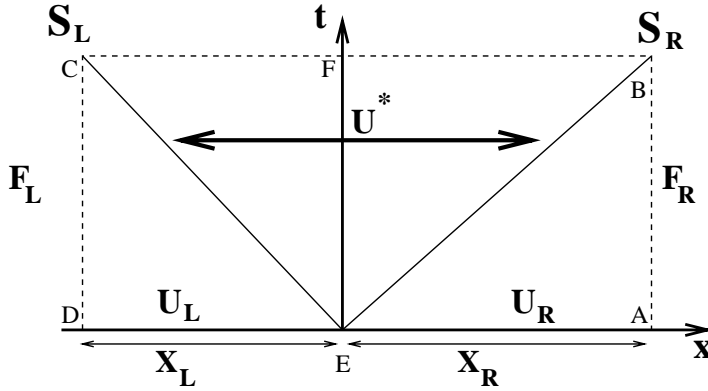


FIG. 2. Simplified Riemann fan with one intermediate state.

Noting that  $x_l = -\Delta t S_L$  and  $x_r = \Delta t S_R$ , an evaluation of (18) over the rectangle  $ABCD$  (see Figure 2) gives the value of  $U^*$  in this region as

$$(21) \quad U^* = \frac{S_R U_r - S_L U_l - (F_r - F_l)}{S_R - S_L}.$$

Since this was determined from the conservation law (18),  $U^*$  represents the mean value of the exact solution over the interval  $(\Delta t S_L, \Delta t S_R)$ .

Evaluating (17) over  $DEFC$  gives the corresponding interface flux as

$$(22) \quad F_{lr}^* = \frac{S_R F_l - S_L F_r + S_L S_R (U_r - U_l)}{S_R - S_L}.$$

In the general case, the interface flux, denoted  $F_{HLL}$ , becomes,

$$(23) \quad F_{HLL} = \begin{cases} F_l & \text{if } S_L > 0, \\ F_{lr}^* & \text{if } S_L \leq 0 \leq S_R, \\ F_r & \text{if } S_R < 0, \end{cases}$$

with  $F_{lr}^*$  given by (22). (It is important to note that one should not attempt to compute the flux directly from  $F = F(U_{HLL})$ , with  $U_{HLL}$  given by (20), since in the subsonic case, the flux  $F(U^*)$  will not be consistent with the integral conservation law (17).)

Finally, the  $F_{HLL}$  flux can be constructed rapidly without the use of logic statements by combining (22),(23) into a single formula,

$$(24) \quad F_{HLL} = t_1 F_r + t_2 F_l - t_3 (U_r - U_l),$$

with

$$t_1 = \frac{\min(S_R, 0) - \min(0, S_L)}{S_R - S_L}, \quad t_2 = 1 - t_1, \quad t_3 = \frac{S_R |S_L| - S_L |S_R|}{2(S_R - S_L)}.$$

This numerical flux satisfies the conservation laws by construction. With appropriate choices for  $S_L$  and  $S_R$ , the HLL Riemann solver automatically satisfies an entropy inequality [3], resolves isolated shocks exactly [8] and preserves positivity [4]. The disadvantage is its inability to exactly resolve isolated contact discontinuities. This is our motivation for the following, two-state HLL approximation.

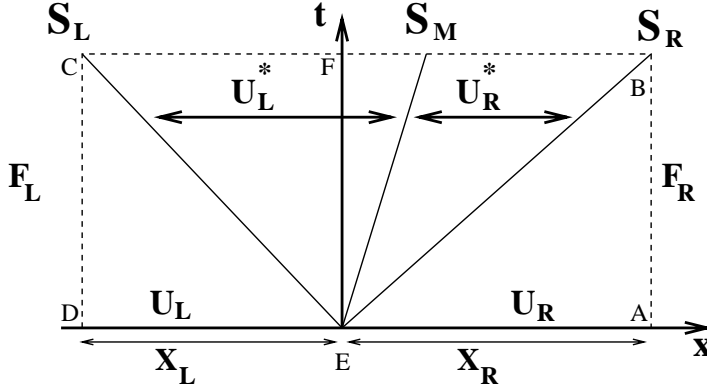


FIG. 3. Simplified Riemann fan with two intermediate states.

**3.2. The HLLC flux.** Consider two averaged intermediate states,  $U_l^*$ ,  $U_r^*$ , separated by the contact wave, whose speed is denoted by  $S_M$  (see Figure 3).

The two-state approximate Riemann solution was defined by Harten, Lax, and van Leer [8] as

$$(25) \quad U_{HLL2} = \begin{cases} U_l & \text{if } S_L > 0, \\ U_l^* & \text{if } S_L \leq 0 < S_M, \\ U_r^* & \text{if } S_M \leq 0 \leq S_R, \\ U_r & \text{if } S_R < 0. \end{cases}$$

The corresponding interface flux, denoted  $F_{HLL2}$ , is defined as

$$(26) \quad F_{HLL2} = \begin{cases} F_l & \text{if } S_L > 0, \\ F_l^* & \text{if } S_L \leq 0 < S_M, \\ F_r^* & \text{if } S_M \leq 0 \leq S_R, \\ F_r & \text{if } S_R < 0. \end{cases}$$

Averaging  $F_{lr}$  from (17) with the equivalent  $F_{lr}$  determined from the integral over the right half of the Riemann fan gives the following expression for the general subsonic flux:

$$(27) \quad F_{lr}^* = \frac{1}{2}[F_l + F_r + (S_R - |S_M|)U_r^* + (S_L + |S_M|)U_l^* - S_L U_l - S_R U_r].$$

Integrating over the rectangle  $ABCD$  and using (21) shows that

$$(28) \quad U^*(S_R - S_L) = U_r^*(S_R - S_M) + U_l^*(S_M - S_L),$$

which simply states that the weighted average of  $U_l^*$ ,  $U_r^*$  must give the mean value of the exact solution,  $U^*$ , between the two acoustic waves.

Harten, Lax, and van Leer [8] and Harten and Lax [7] suggested various ways of computing the  $U_l^*$ ,  $U_r^*$  states from estimates of the flux across the contact line. However, the simplest approach for computing these star states was suggested by Toro, Spruce, and Speares [15], who observed that (ignoring the influence of expansion fans) the particle velocity may be assumed constant between the acoustic waves. Applying the Rankine–Hugoniot conditions across the  $S_L$  wave gives

$$(29) \quad F_l^* = F_l + S_L(U_l^* - U_l).$$

Similarly, the jump relations across the  $S_R$  wave gives

$$(30) \quad F_r^* = F_r + S_R(U_r^* - U_r).$$

Equation (29) may be written as

$$(31) \quad S_L U_l^* - F_l^* = S_L U_l - F_l.$$

For the three-dimensional Euler equations with states  $U_l$ ,  $U_r$  separated by an interface with unit normal vector  $\vec{n}$ , (31) becomes

$$(32) \quad S_L \begin{bmatrix} \rho_l^* \\ \rho_l^* u_l^* \\ \rho_l^* v_l^* \\ \rho_l^* w_l^* \\ e_l^* \end{bmatrix} - \begin{bmatrix} \rho_l^* q_l^* \\ \rho_l^* u_l^* q_l^* + p^* n_x \\ \rho_l^* v_l^* q_l^* + p^* n_y \\ \rho_l^* w_l^* q_l^* + p^* n_z \\ (e_l^* + p^*) q_l^* \end{bmatrix} = S_L \begin{bmatrix} \rho_l \\ \rho_l u_l \\ \rho_l v_l \\ \rho_l w_l \\ e_l \end{bmatrix} - \begin{bmatrix} \rho_l q_l \\ \rho_l u_l q_l + p_l n_x \\ \rho_l v_l q_l + p_l n_y \\ \rho_l w_l q_l + p_l n_z \\ (e_l + p_l) q_l \end{bmatrix},$$

where  $q = un_x + vn_y + wn_z$ .

To determine  $U_l^*$  (and hence  $F_l^*$ ), Toro, Spruce, and Speares [15] made the assumption that

$$S_M = q_l^* = q_r^* = q^c,$$

where  $q^c$  was taken as some estimate of the contact velocity. Our assumption is more specific, in that we insist that

$$(33) \quad S_M = q_l^* = q_r^* = q^*,$$

where  $q^*$  is the average directed velocity between the two acoustic waves. Our choice for the contact wavespeed,  $S_M$ , is therefore to extract the average velocity from the HLL approximation to  $U^*$  (21). This gives the following expression for  $S_M$ :

$$(34) \quad S_M = \frac{\rho_r q_r (S_R - q_r) - \rho_l q_l (S_L - q_l) + p_l - p_r}{\rho_r (S_R - q_r) - \rho_l (S_L - q_l)}.$$

Toro, Spruce, and Speares [15] noted that once  $q_l^*$  is available, (32) can be manipulated to find all remaining components of  $U_l^*$ . Using (33), the first equation in (32) gives

$$(35) \quad \rho_l^* = \rho_l \frac{(S_L - q_l)}{(S_L - S_M)}.$$

Multiplying the second, third, and fourth equations of (32) by  $n_x$ ,  $n_y$ ,  $n_z$ , respectively, and summing gives

$$S_L \rho_l^* S_M - \rho_l^* S_M^2 - p^* = S_L \rho_l q_l - \rho_l q_l^2 - p_l.$$

Using (35), this simplifies to give

$$(36) \quad p^* = \rho_l (q_l - S_L) (q_l - S_M) + p_l.$$

By equating (36) with the corresponding expression for  $p^*$  obtained from the jump conditions across the  $S_R$  wave (30), one can verify that our choice of contact wavespeed (34) always gives  $p_l^* = p_r^*$ . This is consistent with the exact solution in that pressure

is not discontinuous across the contact wave, and this property also simplifies the treatment of the implicit HLLC flux [1].

With  $\rho_l^*$  and  $p^*$  specified,  $(\rho u)_l^*$ ,  $(\rho v)_l^*$ , and  $(\rho w)_l^*$  may be obtained from (32) as

$$(37) \quad (\rho u)_l^* = \frac{(S_L - q_l)\rho_l u_l + (p^* - p_l)n_x}{S_L - S_M},$$

$$(38) \quad (\rho v)_l^* = \frac{(S_L - q_l)\rho_l v_l + (p^* - p_l)n_y}{S_L - S_M},$$

$$(39) \quad (\rho w)_l^* = \frac{(S_L - q_l)\rho_l w_l + (p^* - p_l)n_z}{S_L - S_M}.$$

The final equation of (32) gives

$$(40) \quad e_l^* = \frac{(S_L - q_l)e_l - p_l q_l + p^* S_M}{S_L - S_M}.$$

Any additional, passively transported scalar variable,  $\phi$ , may be determined in the star region from

$$(41) \quad (\rho \phi)_l^* = (\rho \phi)_l \frac{(S_L - q_l)}{(S_L - S_M)}.$$

From equations (35) to (40), the flux vector  $F_l^*$  may be obtained directly from (32). In the case where  $S_M < 0$ , the equations for  $F_r^*$  follow by simply changing the  $l$  or  $L$  subscripts to  $r$  and  $R$ , respectively. Alternatively, once both star states are determined, the subsonic flux (with  $S_M$  of either sign) may be found from (27).

The following section describes the final part of the construction, which involves a suitable choice of the acoustic wavespeeds,  $S_L$  and  $S_R$ .

**4. Acoustic wavespeed estimates.** If the system (11) has  $m$  components, the solution to the Riemann problem consists of states  $U_k$ ,  $k = 0, 1, 2, \dots, m$ , where  $U_0 = U_r$  and  $U_m = U_r$ . These states are separated by waves whose characteristic speeds are denoted (in ascending order) by  $\lambda_1, \lambda_2, \dots, \lambda_m$ . We are interested in estimating  $S_L = \lambda_1$  and  $S_R = \lambda_m$  from the initial data  $U_l, U_r$ . There are three possible situations for the Euler equations. In the first situation,

$$(42) \quad \lambda_k(U_{k-1}) = \lambda_k(U_k)$$

and the  $k$ th wave is a contact discontinuity moving with velocity  $a_k = \lambda_k$ . This situation is analogous to that of the linear wave equation. In the second situation,

$$(43) \quad \lambda_k(U_{k-1}) < \lambda_k(U_k)$$

and the  $k$ th wave is an expansion wave, representing a continuous transition between states  $U_{k-1}$  and  $U_k$ . In the final situation,

$$(44) \quad \lambda_k(U_{k-1}) > \lambda_k(U_k)$$

and the  $k$ th wave is a shock moving with speed  $s$ , where

$$(45) \quad \lambda_k(U_{k-1}) > s > \lambda_k(U_k).$$

It should be emphasized that we cannot compute these intermediate wave states exactly without computing the exact Riemann solution. An excellent review of this

problem and several algorithms for estimating these acoustic wavespeeds are given by Davis [3], who observed that because of relation (43), the expansion-wave velocity can be bounded simply by taking

$$(46) \quad \begin{aligned} S_L &= \lambda_1(U_l), \\ S_R &= \lambda_m(U_r). \end{aligned}$$

This wavespeed algorithm will always underestimate shock velocities because of relation (44). Hence, Davis [3] suggested comparing the maximum and minimum characteristic velocities of both states,  $U_l$  and  $U_r$ :

$$(47) \quad \begin{aligned} S_L &= \min[\lambda_1(U_l), \lambda_1(U_r)], \\ S_R &= \max[\lambda_m(U_l), \lambda_m(U_r)]. \end{aligned}$$

Davis [3] further suggested that one could estimate the shock velocities from an intermediate state based on the Roe average [12]. This was implemented in the following wavespeed algorithm due to Einfeldt et al. [4]:

$$(48) \quad \begin{aligned} S_L &= \min[\lambda_1(U_l), \lambda_1(U^{Roe})], \\ S_R &= \max[\lambda_m(U^{Roe}), \lambda_m(U_r)]. \end{aligned}$$

In general, (48) will be less diffusive than (47) and in the case of an isolated shock, (48) will return the exact shock velocity. Einfeldt et al. [4] state (incorrectly) that (48) are lower and upper bounds for the physical signal velocity. In fact, there remains a possibility that any of the above algorithms may underestimate the shock velocity if either the 1-wave is a shock and

$$(49) \quad \lambda_1(U_l) < \lambda_1(U_r),$$

or the  $m$ -wave is a shock and

$$(50) \quad \lambda_m(U_l) < \lambda_m(U_{m-1}).$$

This can occur in any situation where multiple waves collide in (or collapse from) a single cell. Where multiple waves collapse from a cell (a shock-tube problem, for example) it suffices to use a slightly reduced CFL number until the waves have spread over two or more cells. Where multiple shocks collide in a cell, there appears to be a distinct advantage in computing some kind of intermediate state (such as a Roe average or an arithmetic average which assumes quiescent gas whenever  $q_l$  and  $q_r$  are of opposite sign) in order to pick up the peak pressures at the point of impact which are never seen by (47). In practice, (48) has proved extremely robust, and since this yields the exact velocity for isolated shocks, this is the algorithm we recommend and use throughout the remainder of the paper. These wavespeeds are computed from

$$(51) \quad \begin{aligned} S_L &= \min[q_l - c_l, \tilde{q} - \tilde{c}], \\ S_R &= \max[q_r + c_r, \tilde{q} + \tilde{c}], \end{aligned}$$

where

$$\begin{aligned} \tilde{q} &= \tilde{u}n_x + \tilde{v}n_y + \tilde{w}n_z, \\ \tilde{u} &= (u_l + u_r R_\rho)/(1 + R_\rho), \end{aligned}$$

$$\begin{aligned}\tilde{v} &= (v_l + v_r R_\rho) / (1 + R_\rho), \\ \tilde{w} &= (w_l + w_r R_\rho) / (1 + R_\rho), \\ \tilde{c}^2 &= (\gamma - 1) \left[ \tilde{H} - \frac{1}{2} (\tilde{u}^2 + \tilde{v}^2 + \tilde{w}^2) \right], \\ \tilde{H} &= (H_l + H_r R_\rho) / (1 + R_\rho), \\ R_\rho &= \sqrt{\rho_r / \rho_l},\end{aligned}$$

where  $\gamma$  is the ratio of specific heat capacities and  $H = (e + p)/\rho$  is the enthalpy.

**5. Properties of the numerical flux.** This section motivates our choice of acoustic and contact wavespeed estimates by illustrating three properties of the resulting numerical flux,  $F_{HLLC}$ , defined by the HLLC construction (35)–(40), with wavespeeds (34) and (51).

**5.1. Exact resolution of isolated contacts.** At an isolated contact surface or slip-line

$$(52) \quad q = q_l = q_r,$$

$$(53) \quad p = p_l = p_r.$$

Substituting (52) and (53) into (34) gives

$$S_M = q \left[ \frac{\rho_r(S_R - q) + \rho_l(q - S_L)}{\rho_r(S_R - q) + \rho_l(q - S_L)} \right] = q.$$

From (25) we obtain the corresponding exact solution for a general  $x/t$ :

$$(54) \quad U^* = \begin{cases} U_l & \text{if } x/t < q, \\ U_r & \text{if } x/t > q. \end{cases}$$

Note that this property holds for any choice of acoustic wavespeeds.

**5.2. Exact resolution of isolated shocks.** At an isolated shock wave, the shock velocity,  $s$ , is given by the largest (or smallest) eigenvalue of the Roe matrix [12]. It suffices to consider the case where the shock corresponds to the largest eigenvalue, in which case the exact shock velocity is returned by (51) as  $S_R = s$ .

In this situation, the Rankine–Hugoniot conditions give

$$(55) \quad s(\rho_l - \rho_r) = \rho_l q_l - \rho_r q_r,$$

$$(56) \quad s(\rho_l q_l - \rho_r q_r) = \rho_l q_l^2 + p_l - \rho_r q_r^2 - p_r,$$

$$(57) \quad s(e_l - e_r) = (e_l + p_l)q_l - (e_r + p_r)q_r.$$

Substituting the first two of the above relations into (34) gives

$$S_M = \frac{s\rho_r q_r - S_L \rho_l q_l + s(\rho_l q_l - \rho_r q_r)}{s\rho_r - S_L \rho_l + s(\rho_l - \rho_r)} = \frac{\rho_l q_l (s - S_L)}{\rho_l (s - S_L)} = q_l.$$

Substituting  $S_M = q_l$  into relations (35)–(40) and using the above Rankine–Hugoniot relations gives

$$U_l^* = U_r^* = U_l.$$

Similarly, one obtains  $U_l^* = U_r^* = U_r$ , where the shock is connected with the  $S_L$  wave, yielding the general result

$$(58) \quad U^* = \begin{cases} U_l & \text{if } x/t < s, \\ U_r & \text{if } x/t > s. \end{cases}$$

Note that the exact resolution of isolated shocks relies on the use of the exact wavespeeds for  $S_R$  (or  $S_L$ ) and  $S_M$ , both of which are guaranteed in this specific situation by (51) and (34).

**5.3. Positivity preservation.** This argument is based on the fact that our numerical schemes update values from a convex averaging of the states that appear in the exact or approximate solution to the Riemann problem. A Riemann solver yields a positively conservative scheme iff all the states generated are physically real [4]. This set of physically realistic states is defined as those with positive densities and internal energies:

$$(59) \quad G = \left\{ \begin{bmatrix} \rho \\ \rho u \\ \rho v \\ \rho w \\ e \end{bmatrix}, \quad \rho > 0 \quad \text{and} \quad e - \frac{1}{2}\rho(u^2 + v^2 + w^2) > 0 \right\}.$$

For a positively conservative scheme, if the initial condition is contained in  $G$ , then all subsequently generated states will also lie inside  $G$ . An important result demonstrated by Einfeldt et al. [4] is that no scheme whose interface flux derives from a linearized Riemann solver can be positively conservative. In Eulerian methods this loss of positivity occurs at strong rarefactions, where low values of densities and pressures are generated. (The converse situation exists in Lagrangian methods, where it is strong compressions that may lead to loss of positivity; see Munz [10].)

We require that for all intermediate states,  $U_c$ ,

$$(60) \quad \rho_c > 0,$$

$$(61) \quad e_c - \frac{1}{2}\rho_c(u_c^2 + v_c^2 + w_c^2) > 0.$$

Note that  $U_l$ ,  $U_r$  both lie inside  $G$  by assumption on our initial conditions. We consider now the left star state, with the corresponding results for the right star state following by symmetry. The required conditions become

$$(62) \quad \rho_c = \rho_l^* = \rho_l \frac{(S_L - q_l)}{(S_L - S_M)} > 0,$$

$$(63) \quad e_l^* - \frac{1}{2}\rho_l^*((u_l^*)^2 + (v_l^*)^2 + (w_l^*)^2) > 0.$$

At any rarefaction, algorithm (51) returns a bound for the physical signal velocities. The contact velocity,  $S_M$ , given by (34) is simply the average fluid velocity between these two acoustic waves, hence condition (62) is satisfied since

$$(64) \quad S_L < S_M, \quad S_L < q_l.$$

Using relations (35) to (40) and (64), inequality (63) becomes

$$(q_l - S_L)e_l + p_l q_l - p^* S_M + \frac{\sum_{i=1}^3 (S_L \rho_l u_l^i - \rho_l u_l^i q_l - p_l n_i + p^* n_i)^2}{2\rho_l (S_L - q_l)} > 0,$$

where  $[u^1, u^2, u^3]^T = [u, v, w]^T$  and  $[n_1, n_2, n_3]^T = [n_x, n_y, n_z]^T$ . Rearranging gives

$$\begin{aligned}
 & (q_l - S_L)e_l + p_l q_l - (\rho_l(q_l - S_L)(q_l - S_M) + p_l)S_M \\
 & + \frac{\sum_{i=1}^3 (S_L \rho_l u_l^i - \rho_l u_l^i q_l + \rho_l(S_L - q_l)(S_M - q_l)n_i)^2}{2\rho_l(S_L - q_l)} > 0 \\
 \Rightarrow & (q_l - S_L)e_l + \rho_l(q_l - S_L)(S_M - q_l)S_M - p_l(S_M - q_l) \\
 & - \frac{\rho_l(q_l - S_L)}{2} \left[ \sum_{i=1}^3 (u_l^i + (S_M - q_l)n_i)^2 \right] > 0 \\
 \Rightarrow & (q_l - S_L) \left[ \frac{p_l}{(\gamma - 1)} + \frac{1}{2}\rho_l(u_l^2 + v_l^2 + w_l^2) \right] + \rho_l(q_l - S_L)(S_M - q_l)S_M \\
 & - p_l(S_M - q_l) - \frac{\rho_l(q_l - S_L)}{2} [u_l^2 + v_l^2 + w_l^2 + 2q_l(S_M - q_l) + (S_M - q_l)^2] > 0 \\
 \Rightarrow & \frac{\rho_l}{2}(S_M - q_l)^2 - p_l \frac{(S_M - q_l)}{(q_l - S_L)} + \frac{p_l}{(\gamma - 1)} > 0.
 \end{aligned}$$

This can be rewritten as

$$\frac{\rho_l \alpha^2}{2} - \frac{p_l}{(q_l - S_L)} \alpha + \frac{p_l}{(\gamma - 1)} > 0,$$

where  $\alpha = S_M - q_l$ . We insist that this condition hold for any value of  $\alpha$  by ensuring that the discriminant of the above quadratic is negative. This gives the condition

$$\begin{aligned}
 \frac{p_l^2}{(q_l - S_L)^2} - \frac{2p_l \rho_l}{(\gamma - 1)} < 0, \quad \Rightarrow \sqrt{\frac{(\gamma - 1)p_l}{2\rho_l}} < q_l - S_L, \\
 (65) \quad \Rightarrow S_L < q_l - \beta c_l,
 \end{aligned}$$

where

$$\beta = \sqrt{\frac{\gamma - 1}{2\gamma}}, \quad c_l = \sqrt{\frac{\gamma p_l}{\rho_l}},$$

and this condition is always satisfied by our choice of acoustic wavespeeds (51).

Given the difference in construction of the single- and two-state HLL solvers, it is perhaps slightly surprising to note that this condition on the acoustic velocity is exactly the same as that derived by Einfeldt et al. [4] for the original, single-state HLL Riemann solver (23). Einfeldt et al. [4] suggested modifying the expansion-wave velocities in (51) in order to minimize numerical diffusion in the original HLL scheme, resulting in the following relaxed acoustic wavespeed estimates:

$$\begin{aligned}
 S_L &= \min[q_l - \beta c_l, \tilde{q} - \tilde{c}], \\
 (66) \quad S_R &= \max[q_r + \beta c_r, \tilde{q} + \tilde{c}].
 \end{aligned}$$

We denote by  $F_{HLLCE}$  the numerical flux defined by the HLLC construction (35)–(40) with wavespeeds (34) and (66). The reader should note that with the above choice of wavespeeds,  $S_L$  and  $S_R$  no longer bound the exact expansion-wave velocities, and the entropy inequality demonstrated by Davis [3] no longer holds. Hence, for the present HLLC scheme, we prefer to use Einfeldt et al.'s original estimates (51) unaltered.

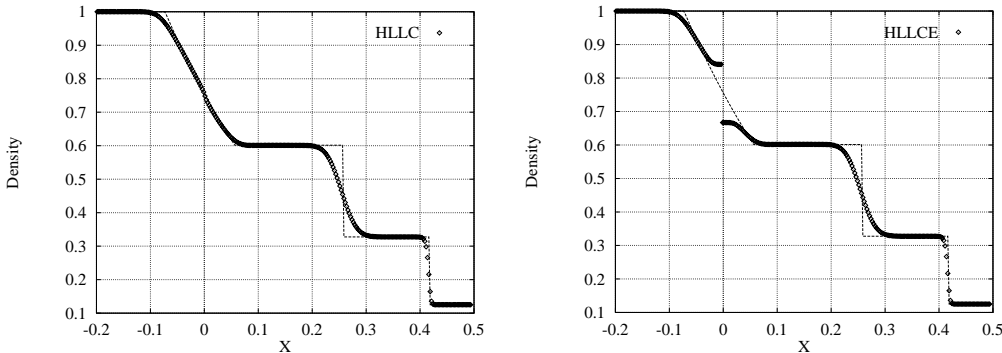


FIG. 4. First-order Godunov scheme using HLLC (left) and HLLCE (right) fluxes.

**6. Some example applications.** In this section we show how the HLLC flux performs with the suggested choice of wavespeeds, (34) and (51). The emphasis is on the behavior of the numerical flux, and therefore we do not give details here of the numerical integration schemes. Where higher-order accuracy is obtained, the same scheme has been used with each numerical flux.

**6.1. Toro's shock-tube problem.** This Riemann problem is a modification of that proposed by Sod [14]. The problem consists of a tube, with a membrane in its center, separating two gases of differing pressure and density, with the gas on the left moving towards the membrane. The membrane bursts at time  $t = 0$ , and a shock wave moves to the right, followed by a contact discontinuity. This problem is so constructed that the left-moving expansion fan is centered on a sonic point.

The initial states to the left and right of the diaphragm are given by

$$(67) \quad U(x, 0) = \begin{cases} U_l & \text{if } x < 0, \\ U_r & \text{if } x \geq 0, \end{cases}$$

where

$$U_l = [1.0, 0.75, 0, 0, 2.5]^T, \quad U_r = [0.125, 0, 0, 0, 0.25]^T.$$

The grid was taken as a uniform mesh of 400 cells in the interval  $-0.5 < x < 0.5$  and the time-step determined from a locally linearized CFL number of 0.5. The solution for each of the methods is illustrated at  $t = 0.2$ , with the dashed line in each figure showing the exact solution to the Riemann problem (67) at this instant.

Figures 4 and 5 show first-order solutions computed with the  $F_{HLLC}$ ,  $F_{HLLCE}$ , and exact Riemann solver fluxes. The HLLCE solution, obtained via the relaxed wavespeed estimates (66), generates an expansion shock almost as large as that which would be obtained from an unmodified Roe scheme [12] (although this effect diminishes with increasing temporal accuracy). The solution computed with the exact Riemann solver produces just a small expansion shock, while the HLLC solution produces nothing more than a slight glitch. The second-order solutions using the exact Riemann solver and HLLC fluxes (shown on the right of Figure 5) are virtually indistinguishable.

**6.2. Mach 3.0 flow over a forward facing step.** This channel flow problem was studied previously by Woodward and Colella [17] and has proved a challenging test case because of the impulsively started supersonic flow around the discontinuity

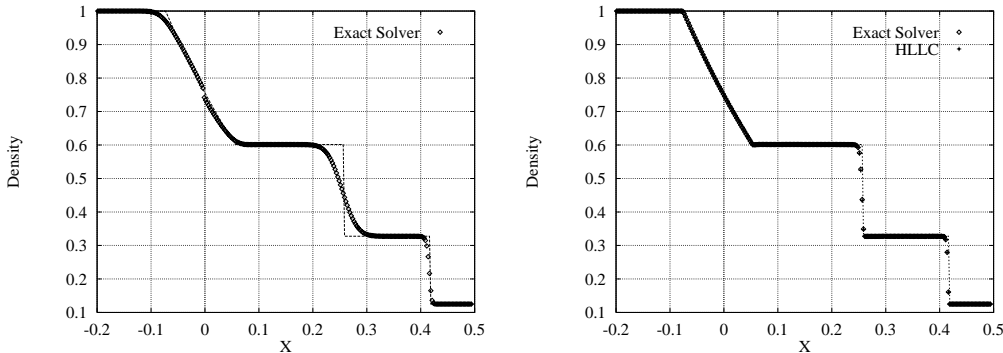


FIG. 5. First-order Godunov scheme using exact Riemann solver (left) and second-order scheme using HLLC and exact Riemann solver fluxes (right).

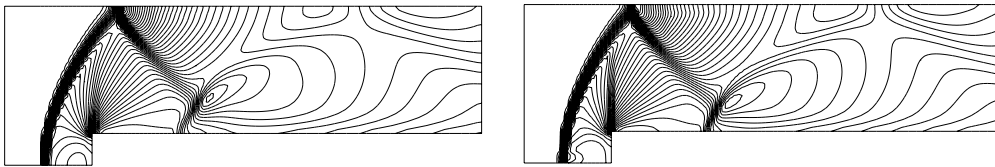


FIG. 6. First-order solutions computed using HLLC (left) and exact Riemann solver fluxes (right).

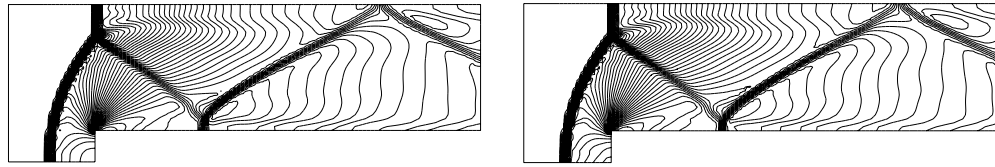


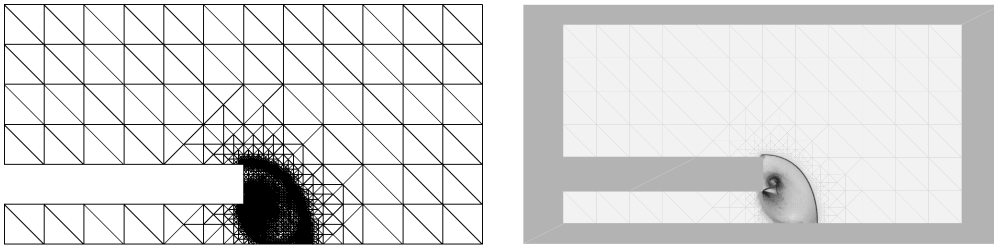
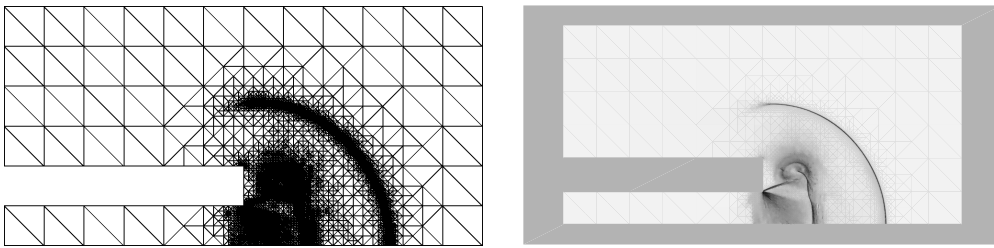
FIG. 7. Second-order solutions computed using HLLC (left) and exact Riemann solver fluxes (right).

at the corner of the step. Each solution was computed on a relatively coarse uniform mesh of 120 by 40 cells, with the time-step determined from a locally linearized Courant number of 0.5. On each of the figures, the density contours are illustrated at  $t = 4.0$ .

Figure 6 shows first-order solutions computed using the  $F_{HLLC}$  and exact Riemann solver fluxes. The solution computed using the exact Riemann solver does a slightly better job of capturing the reflected shock waves, at the expense of a small expansion shock. The second-order solutions in Figure 7 are, again, virtually indistinguishable.

**6.3. A muzzle blast problem.** The final numerical example is that of a muzzle blast, computed using a second-order positivity-preserving scheme using the  $F_{HLLC}$  flux. This muzzle blast problem has previously been simulated numerically by Wang and Widhopf [16] and studied experimentally by Schmidt and Duffy [13].

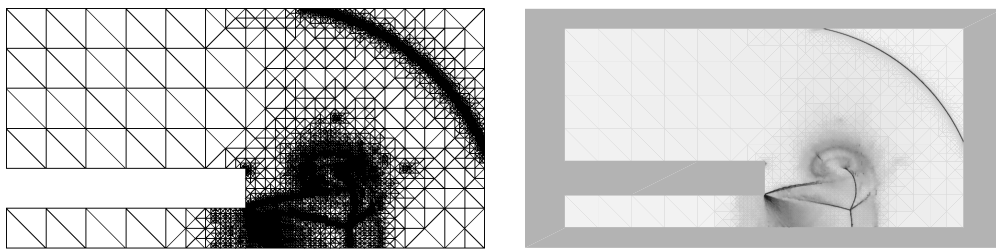
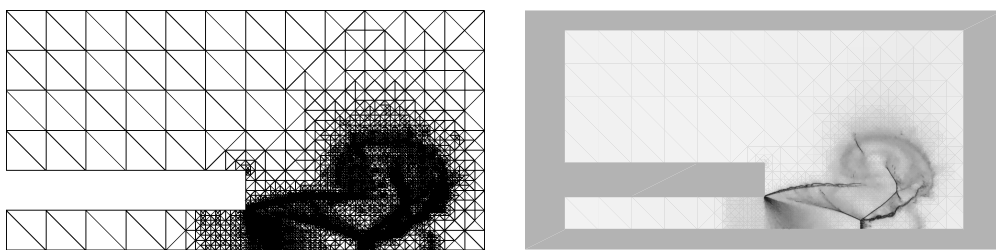
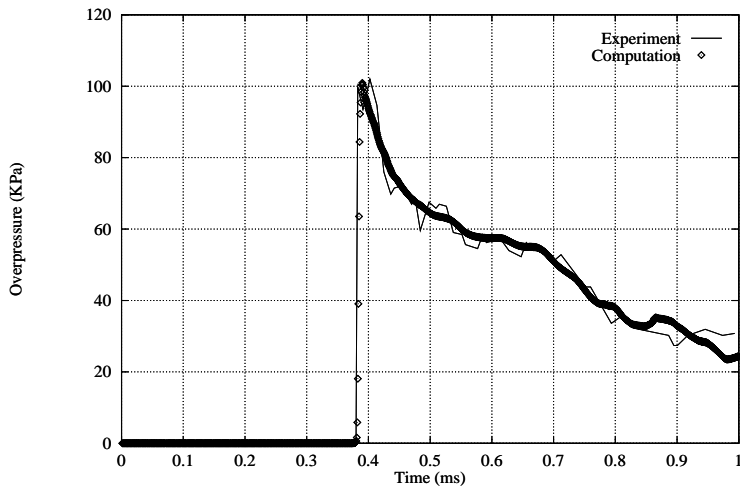
The problem is axisymmetric, and therefore the two-dimensional Euler equations are integrated by solving for the axisymmetric source terms in an operator-splitting sequence. The initial conditions are obtained by applying the Rankine–Hugoniot shock conditions for a weak shock, of shock Mach number 1.76, at the lip of the tube. Time zero is measured from this condition. The equations were solved numerically on

FIG. 8. *Mesh and Schlieren-type snapshots at  $t = 0.2$  ms.*FIG. 9. *Mesh and Schlieren-type snapshots at  $t = 0.5$  ms.*

an unstructured grid which automatically adapts to density gradients in the solution. The time-step was determined from a locally linearized CFL limit of 0.8, and Schlieren-type plots (capable of illustrating weak density gradients) are shown at  $t = 0.2, 0.5, 1.0$ , and  $1.5$  ms.

At time  $t = 0.2$  ms (Figure 8), just before the shock diffracts around the tube, a vortex and slip-line can be seen emanating from the corner of the tube. Later, the initial shock forms an almost spherical blast wave and a Mach disk forms on the axis. At  $t = 0.5$  ms (Figure 9) a recompression shock strengthens and moves towards the tube axis. The slip-line becomes more pronounced, and we see the first appearance of a vortex shock. At  $t = 1.0$  ms (Figure 10) a jet shock meets the recompression shock at a triple point, with the formation of a slip-line. The recompression shock shrinks to form a Mach disk around the axis. At  $t = 1.5$  ms (Figure 11) the initial blast wave has left the domain. The jet shock is prominent below the slip-line and meets the Mach disk at a triple point. A Kelvin–Helmholtz instability is observed at the slip-line downstream of this triple point. Two vortex shocks are now visible, with the lower shock meeting the recompression shock at another triple point. Figure 12 shows a comparison of computed and measured over-pressure at a location on the axis, 1.5 tube diameter lengths downstream of the tube exit. This figure shows reasonable agreement with the experimental results of Schmidt and Duffy [13], with the peak over-pressure agreeing to within 1%. The initial and final meshes contained 570 and 54,536 triangular elements, respectively.

**7. Conclusions.** In this paper we have suggested algorithms for computing the contact and acoustic wavespeeds required for the HLLC approximate Riemann solver of Toro, Spruce, and Speares [15]. We have shown that the resulting two-state HLL Riemann solver will resolve both isolated shock and contact waves exactly. It has also been shown that the proposed choice of wavespeeds guarantees that the method will be positively conservative. In all cases computed, the solutions have been found to be comparable to those produced with an exact Riemann solver, only with a stronger enforcement of the entropy condition across expansion waves.

FIG. 10. *Mesh and Schlieren-type snapshots at  $t = 1.0$  ms.*FIG. 11. *Mesh and Schlieren-type snapshots at  $t = 1.5$  ms.*FIG. 12. *Comparison of computed and measured over-pressures.*

**Acknowledgments.** We are grateful to Professors Tito Toro and James Hyman for a number of useful comments on this paper.

## REFERENCES

- [1] P. BATTEN, U. C. GOLDBERG, AND M. A. LESCHZINER, *Average State Jacobians and Implicit Methods for Compressible Viscous Flow*, Technical Report, Dept. of Mechanical Engineering, UMIST, UK, 1996.
- [2] R. COURANT, E. ISAACSON, AND M. REES, *On the solution of non-linear hyperbolic differential equations*, Comm. Pure Appl Math., 5 (1952), pp. 243–255.
- [3] S. F. DAVIS, *Simplified second-order Godunov-type methods*, SIAM J. Sci. Statist. Comput., 9 (1988), pp. 445–473.

- [4] B. EINFELDT, C. D. MUNZ, P. L. ROE, AND B. SJOGREEN, *On Godunov-type methods near low densities*, J. Comput. Phys., 92 (1991), pp. 273–295.
- [5] S. K. GODUNOV, *A difference method for the numerical calculation of discontinuous solutions of hydrodynamic equations*, Mat. Sb., 47 (1959), p. 271.
- [6] A. HARTEN AND J. M. HYMAN, *Self-adjusting grid methods for one-dimensional hyperbolic conservation laws*, J. Comput. Phys., 50 (1983), pp. 235–269.
- [7] A. HARTEN AND P. D. LAX, *A random choice finite difference scheme for hyperbolic conservation laws*, SIAM J. Numer. Anal., 18 (1981), pp. 289–315.
- [8] A. HARTEN, P. D. LAX, AND B. VAN LEER, *On upstream differencing and Godunov-type schemes for hyperbolic conservation laws*, SIAM Rev., 25 (1983), pp. 35–61.
- [9] P. D. LAX, *Weak solutions of non-linear hyperbolic equations and their numerical computation*, Comm. Pure Applied Math., 7 (1954), pp. 159–193.
- [10] C. D. MUNZ, *On Godunov-type schemes for Lagrangian gas dynamics*, SIAM J. Numer. Anal., 31 (1994), pp. 17–42.
- [11] S. OSHER, *Riemann solvers, the entropy condition and difference approximations*, SIAM J. Numer. Anal., 21 (1984), pp. 217–235.
- [12] P. L. ROE, *Approximate Riemann solvers, parameter vectors and difference schemes*, J. Comput. Phys., 43 (1981), pp. 357–372.
- [13] E. M. SCHMIDT AND S. DUFFY, *Noise from Shock Tube Facilities*, AIAA Paper 85-0049, AIAA, Washington, DC, 1985.
- [14] G. A. SOD, *Numerical Methods in Fluid Dynamics: Initial and Boundary Value Problems*, Cambridge University Press, Cambridge, UK, 1985.
- [15] E. F. TORO, M. SPRUCE, AND W. SPEARES, *Restoration of the contact surface in the HLL Riemann solver*, Shock Waves, 4 (1994), pp. 25–34.
- [16] J. C. T. WANG AND G. F. WIDHOPF, *Numerical simulation of blast flowfields using a high resolution TVD finite volume scheme*, Comput. Fluids, 18 (1990), pp. 103–137.
- [17] P. R. WOODWARD AND P. COLELLA, *The numerical simulation of two-dimensional fluid flow with strong shocks*, J. Comput. Phys., 54 (1984), pp. 115–173.